

# Effect of Anions in Zn-Based Aqueous Electrolyte on Electrochemical Performance of Prussian Blue Analogue

Asis Sethi, Chaithra Rajeev, Anil Kumar U., Parul Sharma, Anurag Prakash Sunda,\* and Vishal M. Dhavale\*

The effect of an anion from the electrolyte salt plays a crucial role in modulating the solvation structure of the cation and the electrochemical performances of the energy storage systems. Herein, the effect of different anions such as chlorides ( $\text{Cl}^-$ ), nitrates ( $\text{NO}_3^-$ ), sulfates ( $\text{SO}_4^{2-}$ ), and their influence on the solvation structure, diffusivity of  $\text{Zn}^{2+}$  cation, redox kinetics, and ion storing behavior of Zn-based Prussian blue analogue (PBA) electrodes are explored. Combining molecular dynamics simulations and experimental observations, the results divulge that different anions can significantly modulate the solvation shell and diffusivity of the cation, thereby influencing the electrochemical properties of the PBA electrodes. Further, increased anion concentration

and its consequences on the aforementioned properties are investigated by employing 6 m water-in-salt electrolyte (WiSE). It is found that in  $\text{ZnCl}_2$ , a moderate  $\text{Zn}^{2+}\text{-Cl}^-$  interaction offers higher ion diffusivity, thereby facilitating more efficient  $\text{Zn}^{2+}$  intercalation into the PBA electrode, resulting highest specific capacity of 56 mAh g<sup>-1</sup> at 2C-rate and the highest coulombic efficiency of 80% in 1 m  $\text{ZnCl}_2$  and shows superior cycling stability in long-term cycling in 6 m-WiSE comparison to other anions. This work highlights the pivotal role of anions in tuning electrolyte molecular structure and its dynamics, ultimately governing cation transport and electrode kinetics in aqueous zinc-ion batteries.

## 1. Introduction

Energy storage devices based on aqueous electrolytes have emerged as sustainable energy systems due to their low cost, safe operation, and easy cell assembly and testing.<sup>[1,2]</sup> For the development of aqueous-based energy storage systems, electrolyte modification strategies have been adopted by many researchers, specifically towards the improvement of specific capacity, stable electrochemical potential window, and cycling stability.<sup>[3–6]</sup> These performance characteristics are primarily dictated by the judicious selection of electrolyte, its concentration, and ionic composition.<sup>[7,8]</sup> For instance, Xiong et al. improved electrode material stability and capacitance by adding sodium ferrocyanide ( $\text{Na}_4\text{Fe}(\text{CN})_6$ ) based electrolyte additive into aqueous electrolyte.<sup>[9]</sup> Generally, in the

case of aqueous electrolytes, the operating potential window is found to be a function of electrolyte concentration.<sup>[10,11]</sup> For example, recently, Sethi et al. demonstrated that increasing the concentration of the aqueous electrolyte improves the potential window of the electrolyte.<sup>[12]</sup> In addition, a thoughtful selection of cation and anion pairs with an appropriate concentration of the electrolyte is necessary in modulating the solvation structure, and the extent of electrostatic potential (ESP) between cation-anion pairs in aqueous electrolyte.<sup>[13,14]</sup> Prior to the selection of an appropriate cation-anion pair for aqueous electrolytes, it is essential to understand their individual role during the charge storage mechanism. Especially, in aqueous metal-ion batteries, cations such as  $\text{Na}^+$ ,  $\text{K}^+$ ,  $\text{Al}^{3+}$ ,  $\text{Zn}^{2+}$ , etc., act as major charge carriers, while anions contribute least.<sup>[15,16]</sup> Furthermore, the anions can also be tuned to be an active charge carrier to achieve the improved potential window during the charge/discharge process in aqueous-based batteries.<sup>[17,18]</sup> The anions can significantly affect the solvation structure and thereby improve the electrochemical stability of aqueous electrolytes. For instance, Sui et al. explored the impact of different sizes of anions in Li-based aqueous electrolytes for the suppression of oxygen evolution reaction and thereby improving the electrolyte stability, by means of modulated hydrogen-bonding characteristics.<sup>[19]</sup> Similarly, Han et al. investigated the influence of various concentrations of anions such as  $\text{TFSI}^-$ ,  $\text{FSI}^-$ ,  $\text{OTf}^-$ , and  $\text{NO}_3^-$  on the structural and dynamic properties of water in supersaturated aqueous Li-based electrolytes, i.e., water-in-salt electrolyte (WiSE).<sup>[20]</sup> In another instance, Li et al. explored the impact of different anions such as  $\text{PF}_6^-$ ,  $\text{BF}_4^-$ ,  $\text{ClO}_4^-$ ,  $\text{TFSI}^-$ , and  $\text{CF}_3\text{SO}_3^-$  on ionic conductivity, charge transfer resistance, and cycling stability in aqueous electrolyte-based batteries.<sup>[21]</sup> All these efforts are put forward to investigate the impact of anions on the monovalent

A. Sethi, C. Rajeev, A. K. U., V. M. Dhavale  
CSIR-Central Electrochemical Research Institute  
CSIR Madras Complex, Taramani, Chennai, Tamil Nadu 600113, India  
E-mail: vishal@cecri.res.in

A. Sethi, C. Rajeev, A. K. U., V. M. Dhavale  
Academy of Scientific and Innovative Research (AcSIR)  
Ghaziabad 201002, India

A. Sethi  
Department of Chemistry  
Bhadrak Autonomous College  
Bhadrak, Odisha 756100, India

P. Sharma, A. P. Sunda  
Department of Chemistry  
J. C. Bose University of Science and Technology, YMCA  
Faridabad 121006, India  
E-mail: anurag@jcboseust.ac.in

 Supporting information for this article is available on the WWW under <https://doi.org/10.1002/batt.202500488>

cation, such as  $\text{Li}^+$ ,  $\text{Na}^+$ , and it remains elusive for multivalent cations, particularly for  $\text{Zn}^{2+}$ . Further,  $\text{Zn}^{2+}$ , owing to its smaller size (0.74 Å), high charge density, and multi-electron system, is more advantageous compared to other systems. Therefore, understanding the effect of anion on attributes like reaction kinetics, ionic conductivity, charge transfer process, and overall electrochemical performances of  $\text{Zn}^{2+}$  is vital for the zinc-ion storage chemistry in aqueous batteries such as dual-ion battery and aqueous zinc-ion battery. In view of this, it is imperative to identify a suitable host material that can accommodate  $\text{Zn}^{2+}$  cations without being affected by the presence of counter anions. The prussian blue analogues (PBAs) would be a critical choice considering their tunable structure and redox properties by the selection of appropriate metal sites and seamless transition between different morphologies due to ion insertion.<sup>[22]</sup> As a notable example, Quin et al., reported PBAs can undergo both compositional ( $\text{MnFe-PBA}$  to  $\text{ZnFe-PBA}$ ) and morphological transition (nano-cubes to nano sheets), resulting in enhanced stability and wettability.<sup>[23]</sup> In addition to the aforementioned properties, the PBAs possessing transition metal ions coordinated with cyanide ( $\text{CN}^-$ ) ligands provide a 3D open framework architecture along with high reversibility and better compatibility in aqueous electrolytes.<sup>[24-26]</sup> The larger roomy interstitial sites of PBAs can facilitate easy diffusion of  $\text{Zn}^{2+}$  insertion/extraction, thereby providing structural stability for studying the influence of different anions on the electrochemical properties, charge storability, and cycling stability during the charge-discharge (CD) process.<sup>[27,28]</sup> Herein, the Zn-based PBA has been considered as a host material to investigate the effect of an anion present in the aqueous electrolytes of  $\text{ZnCl}_2$ ,  $\text{Zn}(\text{NO}_3)_2$ , and  $\text{ZnSO}_4$ . We have studied different configurations of aqueous electrolytes, keeping  $\text{Zn}^{2+}$  as a common cation and different anions such as  $\text{Cl}^-$ ,  $\text{SO}_4^{2-}$ , and  $\text{NO}_3^-$ , with varying concentrations from 1 m (dilute electrolyte) to 6 m (WiSE). Furthermore, the in-depth understanding of the influence of anion identity on electrolyte structure, ion solvation, and molecular dynamics (MD) has been studied theoretically and experimentally. Our findings facilitate the modulation properties of aqueous electrolytes and are advantageous to achieve better charge storage ability in aqueous-based energy storage systems.

## 2. Results and Discussion

The chemical environment of aqueous  $\text{ZnCl}_2$ ,  $\text{Zn}(\text{NO}_3)_2$ , and  $\text{ZnSO}_4$  electrolytes of different anions,  $\text{Cl}^-$ ,  $\text{NO}_3^-$ , and  $\text{SO}_4^{2-}$  was investigated by Fourier-transform infrared spectroscopy (FT-IR) and Raman spectroscopy (Figure 1 and S1, Supporting Information). Figure 1a depicts the ionic sizes and molecular structure of different anions.<sup>[29]</sup> The FT-IR spectra depicted in Figure 1b indicate the shift of the  $-\text{OH}$  bond stretching peak toward the higher wavenumber for the bulkier anion-based electrolyte, i.e.,  $\text{ZnSO}_4$ , in comparison to aq.  $\text{ZnCl}_2$  and  $\text{Zn}(\text{NO}_3)_2$  electrolytes, and the stretching peak position are in order of  $-\text{OH}_{\text{ZnSO}_4}$  ( $3116 \text{ cm}^{-1}$ )  $>$   $-\text{OH}_{\text{ZnCl}_2}$  ( $3080 \text{ cm}^{-1}$ )  $>$   $-\text{OH}_{\text{Zn}(\text{NO}_3)_2}$  ( $3077 \text{ cm}^{-1}$ ). The lower wavenumber of the  $-\text{OH}$  stretching peak in  $\text{Zn}(\text{NO}_3)_2$

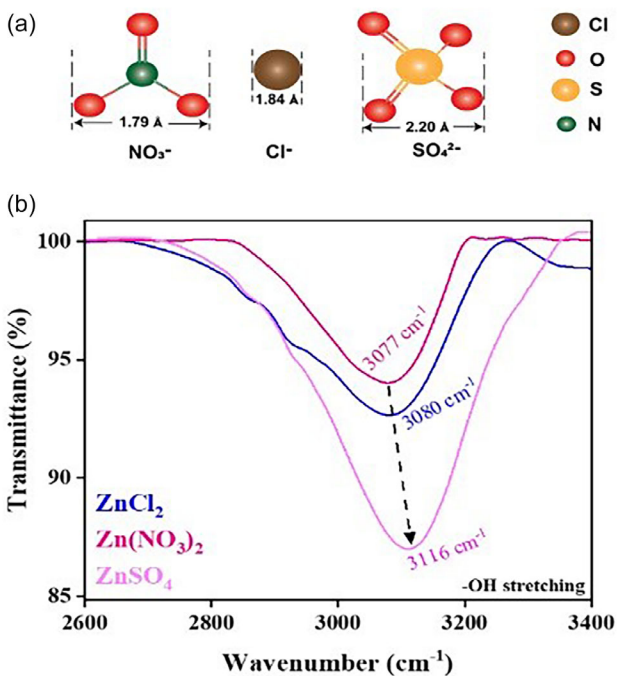


**Figure 1.** a) schematic illustration of ionic sizes and molecular structure of different anions, and b) FT-IR spectrum of  $-\text{OH}$  stretching peak in three different electrolytes of 1 m concentration.

solution suggests that the presence of  $\text{NO}_3^-$  weakens the strength of the O-H bond of water molecules, due to the hydrogen-bonding interaction ( $\text{NO}_3^- \dots \text{H}-\text{O}-\text{H}$ ). Alternatively,  $\text{NO}_3^-$  possesses a lower interaction with the  $\text{Zn}^{2+}$  with an increase in water molecules in the primary solvation shell of the cation, which is in good agreement with the coordination number calculation, presented in Table 1. In contrast, the higher wavenumber of the  $-\text{OH}$  stretching peak in  $\text{ZnSO}_4$  solution suggests that the presence of  $\text{SO}_4^{2-}$  interacts strongly with  $\text{Zn}^{2+}$ , resulting in the strengthening of hydrogen-bonding interaction in water-water coordination in their solvation shell. Whereas,  $-\text{OH}$  bond strength in the presence of  $\text{Cl}^-$  anion, resides between the  $-\text{OH}$  bond strength appeared in  $\text{NO}_3^-$  and  $\text{SO}_4^{2-}$  based aqueous electrolyte (Figure 1b). This could be attributed to the smaller size and lower ionic charge of  $\text{Cl}^-$  in comparison to  $\text{NO}_3^-$  and  $\text{SO}_4^{2-}$ ,

**Table 1.** CN calculated for different atoms in 1m- and 6 m- $\text{ZnCl}_2$ ,  $\text{Zn}(\text{NO}_3)_2$ ,  $\text{ZnSO}_4$ . (cutoff distance (first solvation shell) shown in parentheses).

1 m			
Electrolyte system	$\text{Zn}-\text{O}_w$ [0.3 Å]	$(\text{Cl}, \text{N}, \text{S})-\text{O}_w$ (Cutoff)	$\text{O}_w-\text{O}_w$ [0.33 Å]
$\text{ZnCl}_2$	4.30	6.51 [0.37 Å]	4.11
$\text{Zn}(\text{NO}_3)_2$	4.88	10.72 [0.44 Å]	4.16
$\text{ZnSO}_4$	4.6	13.40 [0.47 Å]	4.18
6 m			
$\text{ZnCl}_2$	2.23	4.72 [0.37 Å]	3.82
$\text{Zn}(\text{NO}_3)_2$	3.09	9.13 [0.44 Å]	3.92
$\text{ZnSO}_4$	3.19	12.52 [0.47 Å]	3.85

which uniformly distributes water molecules by establishing a moderate interaction between  $Zn^{2+}$  and  $Cl^-$ . Further, to delve deeper into the ion–water and water–water interaction in all three different electrolytes, the split-peak fitting Raman spectra is performed (Figure S1, Supporting Information). As shown in Figure S1a, Supporting Information, the deconvolution of the –OH stretching vibration mode of  $ZnSO_4$  into two peaks at 3200 and 3400  $cm^{-1}$  is mainly contributed by the strong and weak hydrogen-bonding between water molecules, respectively.<sup>[30]</sup> Whereas, in the case of  $Zn(NO_3)_2$  and  $ZnCl_2$  solutions, the major portion of the deconvoluted –OH peak is contributed by the hydrogen-bonding with intermediate strength (Figure S1b,c, Supporting Information). Additionally, the peak at a higher wavenumber ( $\approx 3290\text{ cm}^{-1}$ ) in comparison to pure water ( $3200\text{ cm}^{-1}$ ) may be due to the ion-coordinated hydrogen bonding.<sup>[31]</sup> Further, in  $Zn(NO_3)_2$  electrolyte, a larger contribution of very-weak hydrogen-bonding in comparison to  $ZnCl_2$  electrolyte suggests the presence of more bulk water. Overall, FT-IR and Raman spectrum analysis suggested that in aqueous  $ZnCl_2$  electrolyte, the interaction between cation–anion (C–A), water–water (W–W), cation–water (C–W), and anion–water (A–W) is in the intermediate range, whereas in the presence of  $NO_3^-$  in the case of aqueous  $Zn(NO_3)_2$  electrolyte, it reduces the W–W interaction and enhances C–W, A–W interactions. In contrast, the presence of  $SO_4^{2-}$  in aqueous  $ZnSO_4$  electrolyte has enhanced the C–A, and W–W bonding characteristics. Furthermore, it is anticipated that at higher concentrations of the salt in aqueous electrolytes, the chemical interaction and coordination environment of the solvated ion and water molecules may be largely affected and directly influence the solvation structure, diffusion kinetics of ions, and water molecules.<sup>[32,33]</sup> In view of this, a higher concentration of 6 m- $ZnCl_2$ ,  $Zn(NO_3)_2$ , and  $ZnSO_4$  electrolyte, i.e., WiSE, was prepared and investigated by FT-IR and split-peak fitting Raman spectra studies, presented in Figure S2 and S3, Supporting Information. It may be noted that in a 6 m solution, the salt to solvent ratio is greater than 1; hence, it can be termed as a WiSE. At the increased salt concentration of  $ZnCl_2$ ,  $Zn(NO_3)_2$ , and  $ZnSO_4$  in an aqueous electrolyte, i.e., WiSE, the free water content is reduced (Table 1), thereby disrupting the hydrogen bonding network between the water molecules. However, except for 6 m- $Zn(NO_3)_2$  WiSE, the 6 m- $ZnCl_2$  and  $ZnSO_4$  WiSE displayed the blue shift for –OH stretching peak in comparison to their peak position in 1 m electrolytes (Figure S2, Supporting Information), suggesting that no effect of the hydrogen bonding network of the water molecules is seen in 6 m- $Zn(NO_3)_2$  WiSE. A similar observation is also seen in the split-peak fitting Raman spectra. As depicted in Figure S3a, Supporting Information, there is no noticeable alteration in the distribution of different hydrogen-bonding characteristics in the case of 6 m  $Zn(NO_3)_2$  (Figure S3a, Supporting Information). However, a discernible change is evidenced in the case of 6 m  $ZnSO_4$  (Figure S3b, Supporting Information) and  $ZnCl_2$  (Figure S3c, Supporting Information), which is attributed to the contribution from ion-coordinated and weak hydrogen-bonding, respectively. The increase in very-weak hydrogen-bonding characteristics in the case of 6 m  $ZnSO_4$  and  $Zn(NO_3)_2$  compared to

1 m concentration may be correlated to the formation of a close-ion pair (CIP).

Further to gain a deeper understanding of the effect of an anion on  $Zn^{2+}$  solvation structure, a MD simulation study has been carried out. The details of number of molecules used and density of solutions used for the MD simulation study is in Table S1–S3, Supporting Information. The structural characteristics of the solvation shell and the interactions between water molecules in the presence of different anions ( $Cl^-$ ,  $NO_3^-$ , and  $SO_4^{2-}$ ) in 1 m- $ZnCl_2$ ,  $Zn(NO_3)_2$ , and  $ZnSO_4$  were investigated by radial distribution function (RDF) analysis. First, the structural characteristics of water molecules around the  $Zn^{2+}$  cation have been studied, as displayed in Figure 2, a sharp peak appeared at around 2.1 Å, indicating a well-defined first solvation shell around  $Zn^{2+}$ , and a subsequent low peak at 4.2 Å is for the second solvation shell, arising due to the interaction between  $Zn^{2+}$  and the oxygen atom of water ( $g_{Zn-O_{water}}$ ) (Figure 2a). The difference in peak intensity could be attributed to the effect of different anions on the solvation structure of  $Zn^{2+}$ , which can be correlated with water coordination numbers (CNs), presented in Table 1. The CN obtained by integrating the RDF provides an average number of water molecules in the first solvation shell around the  $Zn^{2+}$  ( $Zn^{2+}-H_2O$ ), which is lowest in the 1 m- $ZnCl_2$  solution system (4.3) in comparison to 4.88 and 4.6 in the case of 1 m- $Zn(NO_3)_2$ , and  $ZnSO_4$  solution system, respectively (Table 1). A similar trend of CN for  $Zn^{2+}-H_2O$  is observed in 6 m solution systems (Table 1). In addition, lower ionic size and more localized ionic charge on the  $Cl^-$  ion account for fewer water molecules in the first solvation shell of the  $Zn^{2+}$  cation.<sup>[34]</sup> To get a deeper insight into the arrangement of water molecules in the first solvation shell, cluster analysis is performed (Figure S4, Supporting Information). All the water molecules are situated in the range of 2.0–2.1 Å for a 1 m solution. Water cluster analysis provides an inexplicit information about the difference in water coordination and CN around the  $Zn^{2+}$  and the anions ( $Cl^-$ ,  $NO_3^-$ ,  $SO_4^{2-}$ ). Furthermore, the radial distribution of waters surrounding anions is investigated by studying the RDF of anions and the oxygen atom of water ( $g_{Anions-O_{water}}$ ), shown in Figure 2b. Most of the anions are positioned between the inner and outer solvation shells. The RDF plot clearly demonstrates that  $Cl^-$  ion exhibits the most intense peak at  $\approx 3.2\text{ \AA}$ , whereas  $NO_3^-$ -ion and  $SO_4^{2-}$ -ion engage with water at longer distances, at  $\approx 3.6$  and  $\approx 3.8\text{ \AA}$ , respectively. From this observation, it can be concluded that,  $SO_4^{2-}$  owing to their larger hydrated radii (2.30 Å) and tetrahedral structure, they may appear at a larger distance from their cation counterpart. This phenomenon is opposite in the case of other hydrated anions ( $NO_3^-$ , and  $Cl^-$ ) due to their comparatively smaller radii. CN calculation and cluster analysis (Figure S4, Supporting Information) also support the observation; the lower number of water molecules present around  $Cl^-$ , forming a compact solvation shell, and a higher number of water molecules around  $SO_4^{2-}$  ion (Table 1), accounting for a larger solvation shell. The observations from the cluster analysis are in good agreement with the RDF study (Figure 2b). Combining the results from the RDF study of water around  $Zn^{2+}$  cation and anions around water molecules, the solvation structure of all the anions is

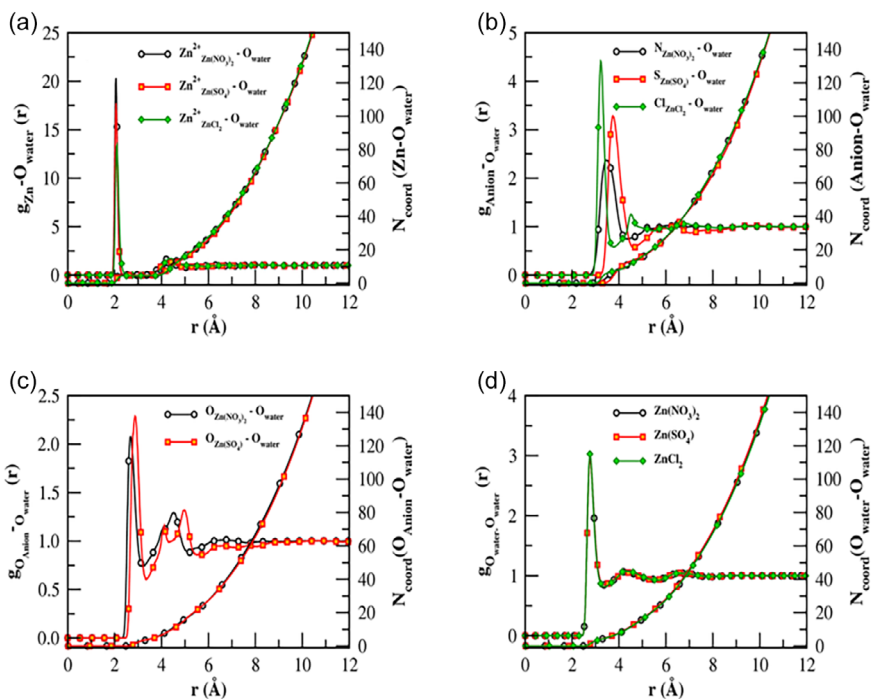
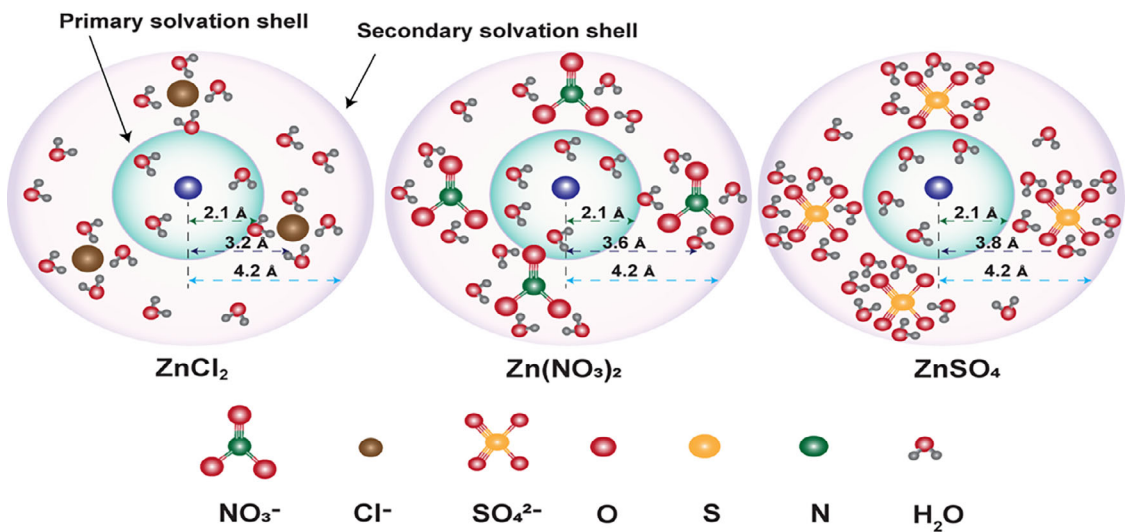


**Figure 2.** RDF along with CN calculated for 1 m electrolytes between, a) Zn and oxygen atom of water ( $\text{O}_\text{water}$ ), b)  $\text{g}_{\text{Anion}-\text{O}_\text{water}}$  (anions and oxygen atom of water), c)  $\text{O}_{\text{Anion}}-\text{O}_\text{water}$  (oxygen atom of anion and oxygen atom of water), d)  $\text{O}_\text{water}-\text{O}_\text{water}$  (oxygen–oxygen atom of water molecules).

schematically illustrated in **Scheme 1**. Further, the  $\text{g}_{\text{O}_{\text{anion}}-\text{O}_\text{water}}$  shows distinct peaks (Figure 2c). A sharp peak is observed around 2.7 Å for  $\text{g}_{\text{O}_{\text{Zn}(\text{NO}_3)_2}-\text{O}_\text{water}}$ , while for  $\text{g}_{\text{O}_{\text{ZnSO}_4}-\text{O}_\text{water}}$ , the peak intensity is relatively high and situated at  $\approx 2.9$  Å, indicating the distribution of water molecules and orientation of “O” atom of the anion toward the inner solvation shell. This aligns with the observation that all the anions are distributed between the inner and outer solvation shells. A characteristic hydrogen-bonding RDF profile is observed for the  $\text{g}_{\text{O}_\text{water}-\text{O}_\text{water}}$  depicted in Figure 2d, with a prominent peak around 2.8 Å for all three-electrolyte solutions. Notably, with increasing concentration of the electrolytes from 1 to 6 M,

the RDF profiles remain unchanged (Figure S5, Supporting Information). Furthermore, detailed information about the distribution of the cation and anion around water molecules is studied by spatial distribution function (SDF) calculation. **Figure 3a-f** shows the SDF maps of  $\text{Zn}^{2+}$  ions around water in 1 and 6 M of  $\text{ZnCl}_2$ ,  $\text{Zn}(\text{NO}_3)_2$ , and  $\text{ZnSO}_4$ . At 1 M, the hydration shell appears well-defined and smooth across all three solutions, showing a characteristic symmetrical ring-type distribution around the water molecule (Figure 3a-c). There is no significant difference in the spatial distribution of  $\text{Zn}^{2+}$  ions around water molecules in different electrolyte solutions of 1 M concentration, suggesting



**Scheme 1.** Schematic illustration of the solvation structure of 1 M— $\text{ZnCl}_2$  (left),  $\text{Zn}(\text{NO}_3)_2$  (middle), and  $\text{ZnSO}_4$  (right).

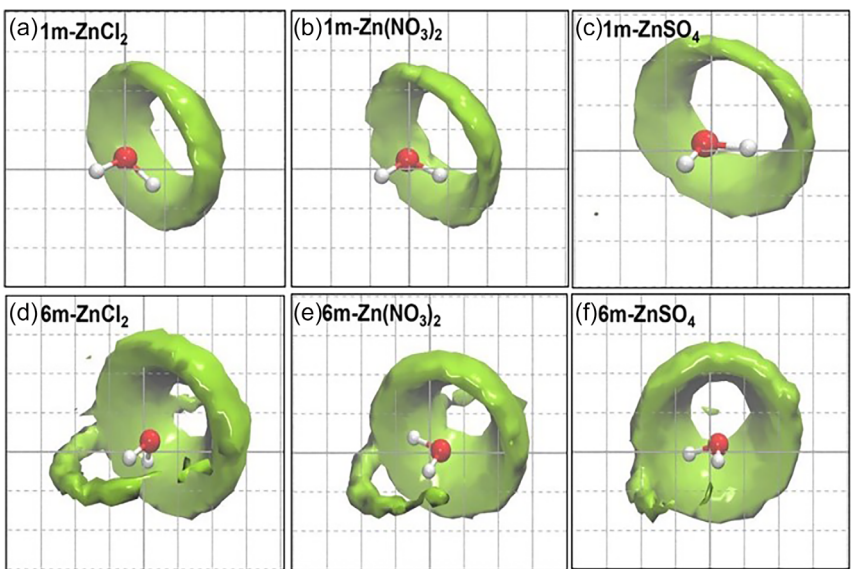


**Figure 3.** SDF calculated for  $Zn^{2+}$  ions around water molecule a) 1m- $ZnCl_2$ , b) 1m- $Zn(NO_3)_2$ , c) 1m- $ZnSO_4$ , d) 6m- $ZnCl_2$ , e) 6m- $Zn(NO_3)_2$ , and f) 6m- $ZnSO_4$  (Color scheme:  $Zn^{2+}$  (Isosurface) green, water (CPK) H-white, O-red) (Isovalue: 0.0025  $\text{\AA}^3$ ).

that at lower concentration, it tends to form solvent-separated ion pairs (SSIP). The formation of SSIP is further supported by the existence of the weak and very-weak hydrogen-bonding in the split-peak fitting Raman spectra of the  $-OH$  peak for all the different electrolytes of 1 m concentration (Figure S1a-c, Supporting Information). However, noticeable differences emerge in the case of 6 m electrolyte solutions.  $Zn^{2+}$  ions in  $ZnCl_2$  (Figure 3d) exhibit the highest spatial density around water. The spatial density of  $Zn^{2+}$  decreases from  $Zn(NO_3)_2$  to  $ZnSO_4$  as depicted in Figure 3e,f, respectively, resulting from the increasing influence of anion size and electrostatic interactions. Notably, this supports the earlier observation from the RDF calculation of stronger ion pair formation between  $Zn^{2+}-SO_4^{2-}$ . Furthermore, at a higher concentration of 6 m, a distorted distribution has been observed, attributed to the decrease in water molecules, making the effect of the anion more noticeable, indicating the formation of CIPs.<sup>[35-37]</sup> Similarly, SDF is performed for different types of anions to investigate anion-water interaction and the distribution of the anions in the solvation shell. Figure 4 shows SDF plots of anions positioned around water molecules. SDF of  $Cl^-$  ion is shown in Figure 4a for a 1 m concentration, depicting a structured toroidal shell around the water molecule, interacting with it through the hydrogen of a water molecule. Whereas in the case of  $NO_3^-$  and  $SO_4^{2-}$  anion, there is comparatively less structured and part-wise distribution (Figure 4b,c) has been observed. This may be due to their distinct structure,  $Cl^-$  being more electronegative and spherical in nature tends to attract water molecules in a uniform way. At the same time,  $NO_3^-$  ion, possessing a trigonal planar shape and delocalized negative charge, is more likely to attract water molecules towards the partial negative charge on the oxygen atom. Similarly,  $SO_4^{2-}$  ion, possessing a tetrahedral structure and bivalent negative charge, is more susceptible than  $NO_3^-$  ion toward water. Further, the charge distribution in all the different electrolyte salts is explored by the electrostatic potential

(ESP) surface analysis (Figure S6, Supporting Information). The ESP surface provides crucial information on electron density distribution and electrostatic properties of varying anions ( $Cl^-$ ,  $NO_3^-$ , and  $SO_4^{2-}$ ) with  $Zn^{2+}$  cation. In the ESP maps, a color scale (red to blue) depicts ranges of ESP of two neighboring cations and anions, with red being the most electron-negative potential (electron-rich) and blue representing the most positive potential (electron-deficient) (Figure S6, Supporting Information). The comparison of the ESP surface shows that charge separation is much higher for monovalent anions ( $Cl^-$  and  $NO_3^-$ ) compared to the bivalent  $SO_4^{2-}$  anion with  $Zn^{2+}$ . Though charge variation is relatively low for  $ZnSO_4$ , it is found to be more prominent relative to the  $Cl^-$  and  $NO_3^-$  anions. As depicted in Figure S6a, Supporting Information,  $ZnCl_2$  possesses a more localized potential uniformly distributed in both the  $Cl^-$  ion around  $Zn^{2+}$ , suggesting lower inter-ionic interaction.  $Zn(NO_3)_2$  shows more delocalized and polarizable ESP, indicating higher interionic interaction than  $ZnCl_2$  (Figure S6b, Supporting Information). The ESP map for  $ZnSO_4$  demonstrates a higher negative potential region compared to others (Figure S6c, Supporting Information), suggesting a higher electrostatic interaction with  $Zn^{2+}$  and solvated water molecules. The velocity autocorrelation function (VACF) analysis provides an in-depth analysis of potential interactions between cation-cation and anion-anion and their influence on dynamical behavior. As demonstrated in Figure S7, Supporting Information, the caging was relatively low for 1 m electrolytes in comparison to 6 m. The influence of anion on caging is clearly seen on  $Zn^{2+}$  ion. The depth of the first minima is found to be more significant for  $Cl^-$  ion, whereas the depth of the first minima is insignificant for  $NO_3^-$  ion. In 6 m WiSE, the solvation structure becomes more disordered due to an increasing number of salt ions and a reduction in solvated water molecules (Figure 4d-f). This is more prominently visible in the case of the  $ZnCl_2$  system, showing a more complex distribution of anions, indicating more

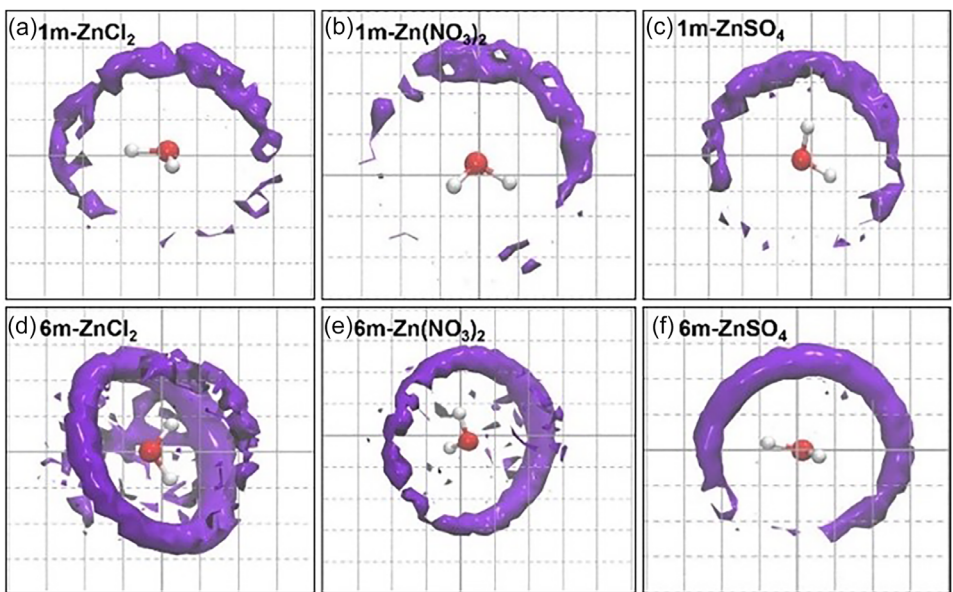


**Figure 4.** SDF calculated for anions around water molecule in 1 m of a)  $\text{ZnCl}_2$ , b)  $\text{Zn}(\text{NO}_3)_2$ , c)  $\text{ZnSO}_4$ , and in 6 m of d)  $\text{ZnCl}_2$ , e)  $\text{Zn}(\text{NO}_3)_2$ , f)  $\text{ZnSO}_4$  (Color scheme: anion (isosurface) violet, water (CPK) H-white, O-red) (Isovalue: 1m-0.001 Å<sup>3</sup> and 6m-0.0021 Å<sup>3</sup>).

frequent  $\text{Cl}^-$ -water interactions, aligning with the FT-IR and Raman observation; In FT-IR spectra, the shifting of  $-\text{OH}$  peak to the lower wavenumber compared to other anionic system (Figure S2, Supporting Information) and in deconvoluted Raman spectra, increase in the strong hydrogen-bonding characteristics (Figure S3c, Supporting Information). In contrast,  $\text{NO}_3^-$  is evidenced with more uniform distribution, and  $\text{SO}_4^{2-}$  ion maintains a closer approach toward water, possibly forming hydrated ion clusters and  $\text{Zn}-\text{SO}_4^{2-}$  ion pair due to its higher negative charge and tetrahedral structure. From the SDF and ESP maps of both the cation and varying anion, it is expected that due to their difference in sizes, geometrical structure, and ionic charge of different anions, they can significantly impact the diffusion behavior of the cation.

Moreover, the diffusion coefficient of the cation is studied by mean square displacement (MSD) calculation performed from the MD simulation [diffusion coefficient for water is provided in Table S4, Supporting Information]. The diffusion coefficients were determined from the slope of the MSD curve (Figure S8, Supporting Information). **Table 2** illustrates the diffusion coefficient of  $\text{Zn}^{2+}$  ions in different electrolyte solutions.  $\text{Zn}^{2+}$  ions exhibited the highest diffusion coefficient in 1 m- $\text{ZnCl}_2$  ( $0.6666 \times 10^{-5}$  cm<sup>2</sup> s<sup>-1</sup>), while 1 m  $\text{ZnSO}_4$  showed the lowest diffusion coefficient of  $0.0383 \times 10^{-5}$  cm<sup>2</sup> s<sup>-1</sup>. SDF analysis of anions surrounded by water molecules and cations depicts that  $\text{Cl}^-$  demonstrates a weaker interaction with  $\text{Zn}^{2+}$  and a stronger interaction with water, resulting in a higher diffusion coefficient of  $\text{Zn}^{2+}$ . The lowest diffusion coefficient of the cation in the presence of  $\text{SO}_4^{2-}$  ion may be due to its stronger interaction with  $\text{Zn}^{2+}$ . As we shifted from dilute to WiSE system, the diffusion coefficient progressively decreased, highlighting the impact of the formation of CIP responsible for the limiting ionic diffusivity. In contrast, the  $\text{Cl}^-$  ions exhibited the highest diffusion coefficient of

**Table 2.** Diffusion coefficients ( $10^{-5}$  cm<sup>2</sup> s<sup>-1</sup>) from MD simulation for  $\text{Zn}^{2+}$  ions.

Electrolyte solutions	1m	6m
$\text{ZnCl}_2$	$0.6666 \pm 0.2120$	$0.0313 \pm 0.0005$
$\text{Zn}(\text{NO}_3)_2$	$0.4021 \pm 0.0712$	$0.0148 \pm 0.0075$
$\text{ZnSO}_4$	$0.0383 \pm 0.0060$	$0.0148 \pm 0.0075$

$0.7744 \times 10^{-5}$  cm<sup>2</sup> s<sup>-1</sup> in comparison to the diffusion coefficient of  $\text{SO}_4^{2-}$  ions ( $0.0397 \times 10^{-5}$  cm<sup>2</sup> s<sup>-1</sup>), at 1 m concentration (Table S5, Supporting Information). To check the diffusive behavior of all the ionic species and water molecules, the first derivative of log (MSD) is plotted against log(t), known as the  $\beta$  (beta) plot. These plots provide insight into the dynamic heterogeneity in the system toward diffusive behavior of species in the electrolyte solutions on a time scale. The results shown in Figure S9, Supporting Information indicates that  $\beta$  values remained close to 1, thereby showing normal diffusion for all the ions, including water molecules at 1 and 6 m WiSE. However, for  $\text{SO}_4^{2-}$  ions, the diffusivity of the cation and anion remains fluctuating. This may be due to the strong ion-pair interaction between  $\text{Zn}^{2+}$  and  $\text{SO}_4^{2-}$ . In addition, different anion group also significantly impacts the solution resistance and hence ionic conductivity (Figure S10, Table S6, Supporting Information). The ionic conductivity of different electrolyte solutions calculated from the EIS measurement by using Equation 1 follows the order of  $\text{Zn}(\text{NO}_3)_2$  ( $0.11$  S cm<sup>-1</sup>)  $>$   $\text{ZnCl}_2$  ( $0.08$  S cm<sup>-1</sup>)  $>$   $\text{ZnSO}_4$  ( $0.05$  S cm<sup>-1</sup>).

$$\sigma = \frac{L}{R_s \cdot A} \quad (1)$$

where  $\sigma$  is the specific ionic conductivity (S cm<sup>-1</sup>),  $L$  is the distance between electrodes (cm),  $R_s$  is the solution resistance ( $\Omega$ ), and  $A$  is the area of the electrode (cm<sup>2</sup>).

Different anions containing electrolytes were employed to assess the impact of anions on the electrochemical properties of the cation. For this purpose, we have employed in-house synthesized zinc-based Prussian blue analogue with rhombohedral structure (PBAR), i.e.,  $\text{Zn}_3\text{Fe}[\text{CN}]_6$ , as the working electrode (details are provided in the Experimental Section, Supporting Information). The cyclic voltammetry (CV) study was conducted to investigate the effect of varying anion ( $\text{NO}_3^-$ ,  $\text{SO}_4^{2-}$ ,  $\text{Cl}^-$ ) on the redox properties of PBAR. Initially, the test is conducted in 1 m- $\text{ZnCl}_2$ ,  $\text{Zn}(\text{NO}_3)_2$ , and  $\text{ZnSO}_4$  electrolytes. In all three different electrolytes, PBAR showed multi-redox behavior, which could be due to the (de)intercalation of the multivalent  $\text{Zn}^{2+}$  cation into the interstitial sites of the PBAR and subsequent change in oxidation state of the redox center ( $\text{Fe}^{3+}/\text{Fe}^{2+}$ ).<sup>[38–41]</sup> However, it is observed that the redox potential shifts with different anion systems, demonstrating the highest redox potential of 0.894 V in aq.  $\text{Zn}(\text{NO}_3)_2$  (for the first redox peak), followed by 0.882, 0.863 V in aq.  $\text{ZnCl}_2$ ,  $\text{ZnSO}_4$ , electrolyte, respectively (Figure 5a). The shifting of the redox potential as a function of anionic species is closely associated with the solvation structure size, diffusivity, and conductivity of the solvated ions.<sup>[42,43]</sup> To further verify the effect of anionic species on the electrochemical properties of PBAR in the presence of cations other than  $\text{Zn}^{2+}$ , a controlled group experiment is electrochemical properties of PBAR in presence of cations other than  $\text{Zn}^{2+}$ , a controlled group experiment is executed by performing CV of PBAR in different cation-based electrolytes (Figure S11, Supporting Information). The CV of PBAR in Na- and Ni-based- $\text{NO}_3^-$ ,  $\text{Cl}^-$ , and  $\text{SO}_4^{2-}$ , demonstrated in Figure S11, Supporting Information. It may be noted that the extent of anionic effect on the electrochemical properties is highly dependent on the size, diffusion coefficient, and the solvation structure of the cation. From the controlled group experiment, it is observed that, unlike  $\text{Zn}^{2+}$ , the presence of  $\text{Na}^+$  and  $\text{Ni}^{2+}$  cations shows no significant anionic effect. The reason behind this intriguing behavior needs to be further investigated. In case of Zn-based aqueous electrolytes, as evidenced by the MD simulation studies, PBAR is expected to show superior electrochemical performance in the presence of  $\text{Cl}^-$  ion due to its compact solvation shell, higher ion diffusion, and low

inter-ionic interaction force of attraction. Notably, it delivered the highest peak current for the redox reaction occurring in aq.  $\text{ZnCl}_2$  electrolyte (Figure 5a). Moreover,  $\text{Zn}^{2+}$  establishes moderate coordination with both  $\text{Cl}^-$  and water molecules, promoting better desolvation energy of the cation. As the coordination environment of the anionic species in the electrolyte varies with concentration, thereby changing the electrochemical properties of the active ion. Hence, to understand the effect of concentration on the redox properties, CV is performed in 6 m WiSE. It is observed that the PBAR demonstrated improved redox potential, persisting multiple redox peaks for all three anionic systems in 6 m WiSE (Figure 5b). The increase in redox potential as a function of concentration of the electrolyte is in accordance with the Nernst Equation (2a and 2b).

$$E = E^\circ + \frac{RT}{nF} \cdot \ln(a_{[\text{cation}]}) \quad (2a)$$

$$E = E^\circ + \frac{RT}{nF} \cdot \ln(c_{[\text{cation}]} \cdot \gamma_{[\text{cation}]}) \quad (2b)$$

where  $E$  is the electrode potential,  $E^\circ$  represents the standard potential,  $R$  and  $T$  are the gas constant and temperature, respectively,  $a_{[\text{cation}]}$ ,  $c_{[\text{cation}]}$ , and  $\gamma_{[\text{cation}]}$  represents the activity, concentration, and activity coefficient of the cation, respectively.

Significant improvement in redox potential is evidenced for both the  $\text{Cl}^-$  and  $\text{NO}_3^-$  anion systems due to an increase in cation activity (Equation 2a and 2b). However, in the case of aq.  $\text{ZnSO}_4$  WiSE, the slightly lower redox potential could be attributed to the formation of CIP due to the presence of  $\text{SO}_4^{2-}$  ion, thereby hindering the ion transfer.<sup>[44]</sup> Further, the influence of different anions on the CD properties of the PBAR is investigated by performing a galvanostatic charge-discharge (GCD) study. From the analysis of computational and experimental studies, it is anticipated that  $\text{NO}_3^-$  ion, being smaller in size and possessing higher ionic conductivity, is more likely to deliver superior CD capacity and ionic reversibility. Figure 6a–c shows the GCD behavior of PBAR in various 1 m electrolyte solutions. GCD curve features two voltage plateaus resembling the CV features. GCD performed

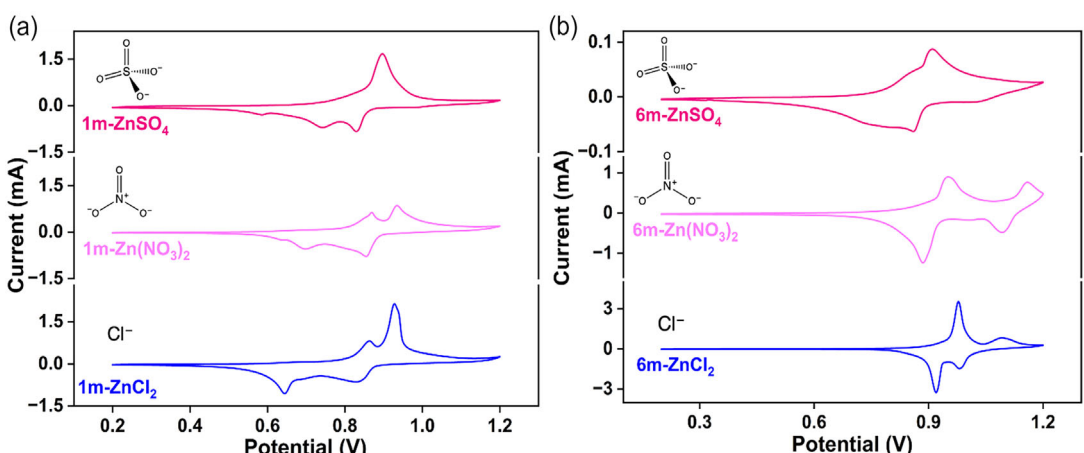
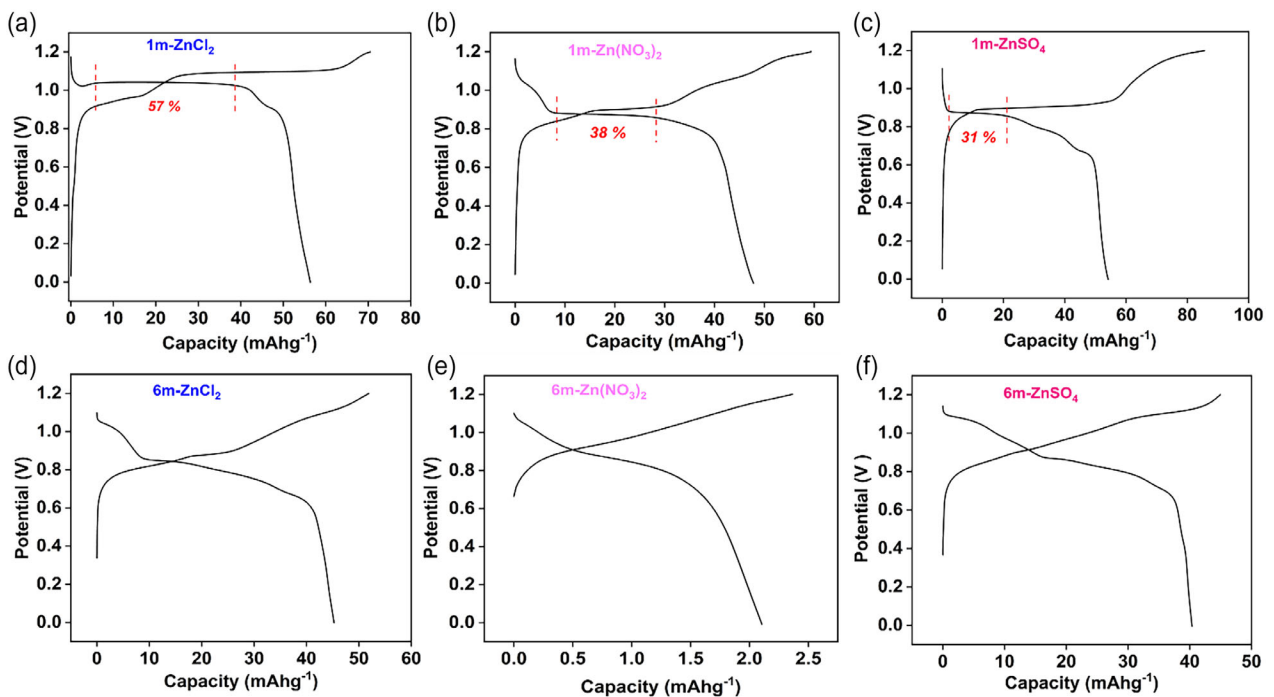


Figure 5. Cyclic voltammogram of PBAR in different electrolyte solutions of  $\text{ZnSO}_4$ ,  $\text{Zn}(\text{NO}_3)_2$ , and  $\text{ZnCl}_2$  in a) 1 m, and b) 6 m WiSE.



**Figure 6.** GCD of PBAR in different electrolyte solutions in 1 m and 6 m concentrations of a,d)  $\text{ZnCl}_2$ , b,e)  $\text{Zn}(\text{NO}_3)_2$ , c,f)  $\text{ZnSO}_4$ , respectively.

at a current rate of 2C (1C rate is defined as  $66 \text{ mA g}^{-1}$ ) demonstrates almost similar discharge specific capacity of 56 and  $54 \text{ mAh g}^{-1}$  in  $\text{ZnCl}_2$  and  $\text{Zn}(\text{NO}_3)_2$ , respectively, whereas it could deliver the lowest discharge capacity of  $48 \text{ mAh g}^{-1}$  in  $\text{ZnSO}_4$  solution. The higher discharge capacity of PBAR in the presence of  $\text{Cl}^-$  and  $\text{NO}_3^-$  may be attributed to their comparatively smaller hydration radii and better diffusion coefficient than  $\text{SO}_4^{2-}$ , thereby providing easy access for the intercalation into interstitial sites of PBAR. Further voltage plateau, which signifies the different electrochemical processes occurring during the CD process, and can provide information on the charge transfer kinetics. Since, lower the activation polarization, the faster will be the charge transfer at the electrode. As illustrated in Figure 6a, the major contribution to the discharge capacity is from a flat voltage plateau in the case of  $\text{Cl}^-$  anionic system, i.e., 57%, suggesting PBAR can get higher usable capacity at a relatively stable potential and good reversibility in  $\text{ZnCl}_2$  electrolyte in comparison to 38 and 31% in the case of 1 m  $\text{Zn}(\text{NO}_3)_2$ , and  $\text{ZnSO}_4$  electrolytes. The lowest contribution of 31% in  $\text{SO}_4^{2-}$  anionic system (Figure 6c), correlating with the higher solution resistance and hence slower ion transfer kinetics, resulting in the higher activation polarization.<sup>[21]</sup> This observation also correlates with the poor coulombic efficiency (CE) of 63% observed in the case of  $\text{ZnSO}_4$  (Figure 6c), while in the presence of  $\text{Cl}^-$  and  $\text{NO}_3^-$  systems, the CE value is around 80% (Figure 6a,b). The higher ionic reversibility in aq.  $\text{Zn}(\text{NO}_3)_2$  and  $\text{ZnCl}_2$  can be correlated to the smaller ionic size, lower ion-pair interaction, higher ionic conductivity, and lower (de)solvation energy compared to  $\text{SO}_4^{2-}$ . To evaluate the performance in WiSE, a GCD study of PBAR is performed in 6 m (Figure 6d-f). The PBAR in  $\text{Zn}(\text{NO}_3)_2$  WiSE almost failed to perform (Figure 6e),

whereas in  $\text{ZnCl}_2$  WiSE, PBAR delivered a higher discharge capacity of  $45 \text{ mAh g}^{-1}$  (Figure 6d) in the first cycle compared to  $40 \text{ mAh g}^{-1}$  in  $\text{ZnSO}_4$  WiSE (Figure 6f). This difference in charge storage behaviour is due to the solvation structure modification, with an increase in concentration of salt, SSIP might be getting converted into CIP.<sup>[44]</sup> In long cycling performance, the PBAR in aq.  $\text{ZnCl}_2$  outperforms, and in aq.  $\text{ZnSO}_4$  in terms of capacity retention, and with similar CE (Figure S12 and S13, Supporting Information). In the 50th cycle, it could retain 69% of capacity with CE of 97% in  $\text{ZnCl}_2$ , whereas in the case of  $\text{ZnSO}_4$ , it could retain the capacity of 67%, and CE of 96% is observed. Overall, PBAR in the presence of  $\text{Cl}^-$ , delivers superior performance than the other two anionic systems in WiSE. The intermediate anionic size, spherical shape, higher ion diffusion, and balanced cation-anion interaction in the presence of  $\text{Cl}^-$ , are found to be a beneficial choice for achieving higher electrochemical performance of PBAR in chloride-based anionic systems and underscore the effect and impact of the anions on the overall battery performance. Additionally, considering the cost and environmental friendliness of different anions ( $\text{Cl}^-$ ,  $\text{SO}_4^{2-}$  and  $\text{NO}_3^-$ ) and their overall impact on the battery is tabulated in Table S7, Supporting Information. Chloride-based anionic salts provide cost-effective and environmentally friendly solutions when used in lower concentrations.<sup>[45]</sup>

### 3. Conclusion

The solvation shell structure of  $\text{Zn}^{2+}$  is significantly influenced by the presence of different anions, affecting the cation's mobility,

desolvation energy, and electrochemical performance of PBAR, as revealed by experimental and theoretical analysis. From the CN calculation and SDF analysis, it is found that in  $\text{ZnCl}_2$  solution, solvated  $\text{Zn}^{2+}$  contains a lesser number of water molecules, arranged in a more uniform manner. Further,  $\text{Zn}^{2+}$  cation shows moderate interactions with  $\text{Cl}^-$ , facilitating higher ion diffusion. Whereas, in  $\text{ZnSO}_4$  electrolyte, due to  $\text{SO}_4^{2-}$  anion's larger hydrated radii, stronger electrostatic interaction with cation and water molecules demonstrated slower ion diffusion. Interestingly, in  $\text{Zn}(\text{NO}_3)_2$ ,  $\text{NO}_3^-$  shows slightly stronger interaction with water molecules but higher ion diffusion than  $\text{SO}_4^{2-}$ . The effect of concentration on solvation structure was investigated by employing 6 m WiSE. While moving from a diluted solution to WiSE, there is a profound alteration in solvation structure as evidenced by SDF analysis. Finally, among all three different electrolytes, i.e.,  $\text{ZnCl}_2$ ,  $\text{Zn}(\text{NO}_3)_2$ , and  $\text{ZnSO}_4$ , in  $\text{ZnCl}_2$ , more efficient  $\text{Zn}^{2+}$  intercalation into the PBAR electrode is observed, resulting in the highest specific capacity of 56  $\text{mAh g}^{-1}$  at 2C-rate and the highest CE of 80% in 1 m  $\text{ZnCl}_2$  and displayed the better long-term cycling stability. This work highlights the pivotal role of anions in tuning electrolyte structure and dynamics, ultimately governing cation transport and electrode kinetics in aqueous zinc-ion systems.

## Supporting Information

Experimental details and computational details are in the Electronic Supplementary Information.

## Acknowledgements

A.S., C.R., A.K.U., and V.M.D. acknowledge the Director, Central Electrochemical Research Institute (CECRI) and Scientist-in-charge, CECRI, CSIR Madras Complex, Chennai, for all the help and support. V.M.D. acknowledges the CSIR and Anusandhan National Research Foundation (ANRF)-SERB for the HCP-44 and SERB-CRG/2021/004395 Grant, respectively. A.K.U. and P.S. acknowledges CSIR-SRF, and -JRF, respectively for the fellowship support. A.P.S. acknowledges the ANRF for the SERB-CRG/2022/001938 Grant. CECRI Contribution Number: CECRI/PESVC/Pubs./2025-067.

## Conflict of Interest

The authors declare no conflict of interest.

## Author Contributions

**Asis Sethi:** design of work, data collection, processing the experimental data, manuscript drafting, etc., **Chaithra Rajeev:** sample synthesis, electrode fabrication and electrochemical testing. **Anil Kumar U.:** re-testing and data analysis. **Parul Sharma** and **Anurag Prakash Sunda:** modeling and simulation study, manuscript editing/corrections, funding acquisition. **Vishal M. Dhavale:** conceptualization, critical inputs on work and experimentation

plans, manuscript editing/correction, supervision, and funding acquisition.

## Data Availability Statement

The data that support the findings of this study are available from the corresponding author upon reasonable request.

**Keywords:** aqueous battery · effect of anion · molecular dynamics simulation · Prussian blue analogue · zinc ion storage

- [1] T. Bertaglia, C. M. Costa, S. Lanceros-Méndez, F. N. Crespiho, *Mater. Adv.* **2024**, *5*, 7534.
- [2] A. M. Adeyinka, O. C. Esan, A. O. Ijaola, P. K. Farayibi, *Sustain. Energy Res.* **2024**, *11*, 26.
- [3] J. O. G. Posada, A. J. R. Rennie, S. P. Villar, V. L. Martins, J. Marinaccio, A. Barnes, C. F. Glover, D. A. Worsley, P. J. Hall, *Renew. Sustain. Energy Rev.* **2017**, *68*, 1174.
- [4] T. Xiong, Y. Guo, X. Wang, *Adv. Funct. Mater.* **2025**, *35*, 2421240.
- [5] T. Liu, X. Dong, B. Tang, R. Zhao, J. Xu, H. Li, S. Gao, Y. Fang, D. Chao, Z. Zhou, *J. Energy Chem.* **2024**, *98*, 311.
- [6] R. Zhao, X. Dong, P. Liang, H. Li, T. Zhang, W. Zhou, B. Wang, Z. Yang, X. Wang, L. Wang, Z. Sun, F. Bu, Z. Zhao, W. Li, D. Zhao, D. Chao, *Adv. Mater.* **2023**, *35*, 2209288.
- [7] J. Yi, Y. Xia, *MRS Energy Sustain.* **2022**, *9*, 106.
- [8] H. Ahn, D. Kim, M. Lee, K. W. Nam, *Commun. Mater.* **2023**, *4*, 37.
- [9] Q. Xiong, C. Xiong, Q. Zhou, M. Shen, J. Song, M. Zhao, Y. Zhang, M. An, Y. Ni, *Small Methods* **2025**, *9*, e2401254.
- [10] D. Dong, C.-X. Zhao, X. Zhang, C. Wang, *Adv. Mater.* **2025**, 2418700, <https://doi.org/10.1002/adma.202418700>.
- [11] L. Suo, O. Borodin, T. Gao, M. Olguin, J. Ho, X. Fan, C. Luo, C. Wang, K. Xu, *Sci. 2015*, *350*, 938.
- [12] A. Sethi, U. A. Kumar, V. M. Dhavale, *ChemPhysChem* **2023**, *24*, e202300098.
- [13] J. Han, A. Mariani, S. Passerini, A. Varzi, *Energy Environ. Sci.* **2023**, *16*, 1480.
- [14] W. Deng, G. Li, X. Wang, *Adv. Funct. Mater.* **2024**, *34*, 2405012.
- [15] Y. S. Byeon, H. B. Lee, Y. Hong, H. Kim, Y.-J. Kim, W. Cho, M.-S. Park, *ACS Appl. Mater. Interfaces* **2025**, *17*, 9322.
- [16] Y. Zhang, R. Cao, C. Ouyang, L. Jiang, Y. Wang, M. Yang, H. Xia, *J. Mater. Chem. A* **2025**, *13*, 3973.
- [17] G. Li, D. Li, M. Lei, C. Li, *Adv. Energy Mater.* **2025**, *15*, 2404282.
- [18] Q. Liu, Y. Wang, X. Yang, D. Zhou, X. Wang, P. Jaumaux, F. Kang, B. Li, X. Ji, G. Wang, *Chem* **2021**, *7*, 1993.
- [19] Y. Sui, A. M. Scida, B. Li, C. Chen, Y. Fu, Y. Fang, P. A. Greaney, T. M. O. Popp, D. Jiang, C. Fang, X. Ji, *Angew. Chemie Int. Ed.* **2024**, *63*, e202401555.
- [20] S. Han, *RSC Adv.* **2019**, *9*, 609.
- [21] J. Li, J. Hao, Q. Yuan, R. Wang, F. Marlton, T. Wang, C. Wang, X. Guo, G. Wang, *Carbon Energy* **2024**, *6*, e518.
- [22] Y. Shi, B. Yang, G. Song, Z. Chen, M. Shakouri, W. Zhou, X. Zhang, G. Yuan, H. Pang, *Angew. Chemie Int. Ed.* **2024**, *63*, e202411579.
- [23] Y. Qian, G. Chang, C. Huang, Y. Yang, Y. Hao, Q. Tang, A. Hu, Y. Li, X. Chen, *Chem. Eng. J.* **2025**, *503*, 158392.
- [24] Y. Li, J. Zhao, Q. Hu, T. Hao, H. Cao, X. Huang, Y. Liu, Y. Zhang, D. Lin, Y. Tang, Y. Cai, *Mater. Today Energy* **2022**, *29*, 101095.
- [25] H. Yao, Y. Gao, X. Lin, H. Zhang, L. Li, S. Chou, *Adv. Energy Mater.* **2024**, *14*, 2401984.
- [26] L.-L. Zhao, Y.-H. Zhao, Y.-M. Wu, P.-F. Wang, Z.-L. Liu, Q.-Y. Zhang, J. Shu, T.-F. Yi, *Energy Storage Mater.* **2025**, *78*, 104299.
- [27] J. Yin, J. Wang, M. Sun, Y. Yang, J. Lyu, L. Wang, X. Dong, C. Ye, H. Bao, J. Guo, B. Chen, X. Zhou, L. Zhai, Z. Li, Z. He, Q. Luo, X. Meng, Y. Ma, J. Zhou, P. Lu, Y. Wang, W. Niu, Z. Zheng, Y. Han, D. Zhang, S. Xi, Y. Yuan, B. Huang, P. Guo, Z. Fan, *Nat. Commun.* **2025**, *16*, 370.
- [28] H. Yi, R. Qin, S. Ding, Y. Wang, S. Li, Q. Zhao, F. Pan, *Adv. Funct. Mater.* **2021**, *31*, 2006970.
- [29] H. K. Roobottom, H. D. B. Jenkins, J. Passmore, L. Glasser, *J. Chem. Educ.* **1999**, *76*, 1570.
- [30] Q. Sun, C. Qin, *Chem. Geol.* **2011**, *283*, 274.
- [31] H. Ge, Y. Zhao, H. Yang, M. Wang, *Spectrochim. Acta A Mol. Biomol. Spectrosc.* **2022**, *267*, 120543.

- [32] X. Li, X. Wang, L. Ma, W. Huang, *Adv. Energy Mater.* **2022**, *12*, 2202068.
- [33] Y. S. Badyal, A. C. Barnes, G. J. Cuello, J. M. Simonson, *J. Phys. Chem. A* **2004**, *108*, 11819.
- [34] D. Li, T. Sun, T. Ma, W. Zhang, Q. Sun, M. Cheng, Z. Zha, W. Xie, Z. Tao, *Adv. Funct. Mater.* **2024**, *34*, 2405145.
- [35] P. D'Angelo, V. Migliorati, A. Gibiino, M. Busato, *Inorg. Chem.* **2022**, *61*, 17313.
- [36] K. J. Naidoo, A. S. Lopis, A. N. Westra, D. J. Robinson, K. R. Koch, *J. Am. Chem. Soc.* **2003**, *125*, 13330.
- [37] D. A. C. da Silva, C. M.J.Pinzón, A. Messias, E. E. Fileti, A. Pascon, D. V. Franco, L. M. Da Silva, H. G. Zanin, *Mater. Adv.* **2022**, *3*, 611.
- [38] Z.-X. Zhu, Z.-W. Lin, Z.-W. Sun, P.-X. Zhang, C.-P. Li, R. Dong, H.-W. Mi, *Rare Met.* **2022**, *41*, 3729.
- [39] L. Zhang, L. Chen, X. Zhou, Z. Liu, *Adv. Energy Mater.* **2015**, *5*, 1400930.
- [40] L. Zhang, L. Chen, X. Zhou, Z. Liu, *Sci. Rep.* **2015**, *5*, 18263.
- [41] Y. Fan, X. Yu, Z. Feng, M. Hu, Y. Zhang, *Molecules* **2022**, *27*, 5387.
- [42] K. Park, D.-M. Kim, K.-H. Ha, B. Kwon, J. Lee, S. Jo, X. Ji, K. T. Lee, *Adv. Sci.* **2022**, *9*, 2203443.
- [43] G. Leverick, Y. Shao-Horn, *Adv. Energy Mater.* **2023**, *13*, 2204094.
- [44] S. Zhou, X. Meng, C. Fu, D. Xu, J. Li, Q. He, S. Lin, S. Liang, Z. Chang, A. Pan, *Small* **2023**, *19*, 2303457.
- [45] C.-M. Geilfus, *Environ. Exp. Bot.* **2019**, *157*, 299.

---

Manuscript received: June 27, 2025

Revised manuscript received: August 14, 2025

Version of record online:

---